Proceedings of the 2nd Marine Energy Technology Symposium
METS2014
April 15-18, 2014, Seattle, WA

CONTROL OF A HELICAL CROSS-FLOW CURRENT TURBINE

Robert Cavagnaro
University of Washington, NNMREC
Seattle, WA, USA

Brian Fabien
University of Washington, NNMREC
Seattle, WA, USA

Brian Polagye[1]
University of Washington, NNMREC
Seattle, WA, USA

[1]Corresponding author: bpolagye@uw.edu, (206) 543 7544

ABSTRACT

Adaptive control strategies utilizing preview information of upstream velocity are promising approaches for enhancing performance and reducing loads on hydrokinetic turbines. A control scheme relating a turbine's characteristic performance curve and rotation rate to an optimal torque setpoint is implemented experimentally and in simulation for a laboratory-scale helical cross-flow turbine. Energy extraction performance for schemes employing adaptive/preview techniques is compared to performance under constant speed and non-adaptive control. Results in simulation indicate significant improvement over constant speed operation and modest improvement over non-adaptive strategies. Experimental results for adaptive strategies are comparable to non-adaptive strategies, due to uncertainty in instantaneous performance curves.

INTRODUCTION

The current state of the art of development of marine hydrokinetic (MHK) energy conversion devices exhibits a wide degree of variability [1]. As designs for systems mature towards commercialization, advanced control strategies are of interest to optimize performance. Common approaches for control of marine current turbines involve the strategy of Maximum Power Point Tracking (MPPT), a feedback control scheme targeting operation at a single optimal point based on a device's characteristic performance curve, utilizing measurements of rotation rate, power generation, and inflow velocity [2,3,4]. Other strategies such as gain scheduled control have been developed to allow systems to maintain robust operation and adapt to changing conditions [5].

Technical similarities between wind and MHK turbines allow wind turbine control strategies to be leveraged. Among these are strategies that make use of information describing the resource in advance of its interaction with the turbine. Such "feedforward" or "preview" control schemes have the potential to optimize system efficiency and mitigate excessive loads [6,7]. In wind applications, these upstream measurements are often difficult to obtain because of both the geometric scale of a wind turbine rotor and limitations of technologies available for remote measurement. For MHK applications, acoustic techniques (e.g., Doppler current profiling) can obtain upstream information more easily and rotor scales are smaller.

A preview-based variable-speed turbine control strategy is developed to maintain optimal performance of a fixed-pitch helical cross-flow turbine. Three variations of the scheme are implemented experimentally at the laboratory scale. These strategies are simulated numerically and compared to a simulation of operation at constant rotation rate. Performance, benefits, and challenges associated with experimental control implementation are discussed.

METHODOLOGY

Turbine and Test Rig Description

The four-bladed, cross-flow helical turbine (Figure 1) is intended for operation in low to moderate currents to provide power for autonomous oceanographic instrumentation deployments [8]. Turbine rotor parameters are given in Table 1.

The high solidity (ratio of the total blade chord length to rotor circumference) of the turbine allows self-starting at low speed, but reduces overall efficiency and rotation rate [8]. The laboratory test rig consists of an optical encoder to measure angular position used to determine rotation rate (ω), a controllable particle brake to provide a resistance to rotation, a reaction torque cell to measure the torque resisting rotation, and an Acoustic Doppler

TABLE 1. MICROPOWER ROTOR PARAMETERS

Parameter	Value
Blade profile	NACA 0018
Number of blades	4
Turbine diameter (D)	17.2 cm
Turbine height (H)	23.4 cm
Turbine aspect ratio	1.36
Helical pitch angle	60°
Blade chord length	4.05 cm
Blade thickness	0.73 cm
Solidity ratio	0.30

Velocimeter (ADV) positioned seven turbine diameters upstream to measure the free-stream velocity (U_∞). Flume velocity is controlled by an adjustable recirculation pump frequency. The torque measurement is the sum of applied brake control torque, (τ_c), and torques associated with bearing friction, vibration, and other losses, (τ_L). For experimental testing, it is assumed τ_c is much greater than τ_L, and the latter is neglected.

Turbine and flume dimensions leads to an average blockage ratio, defined as the ratio of the turbine and support frame projected area to the working cross-sectional area of the flume, of 15%. Blade-chord Reynolds numbers achieved during experiments are in a transitional range from $2x10^4$ to $3x10^4$. The range of Froude number based on an average water depth of 47 cm is 0.12 – 0.15. Flume turbulence intensity under steady-flow conditions, defined as the ratio of the standard deviation of velocity to the mean velocity, is approximately 4%.

Performance Characteristics

The performance of a hydrokinetic turbine is defined by a characteristic curve relating the coefficient of performance (ratio of produced to available power) (C_P) to the tip speed ratio (λ), defined as,

$$C_p = \frac{\tau\omega}{\frac{1}{2}\rho A {U_\infty}^3} \quad (1)$$

$$\lambda = \frac{\omega R}{U_\infty} \quad (2)$$

where R is the turbine radius, A is the projected area (DH), τ is the hydrodynamic torque produced by the turbine, and ρ is the fluid density. Ideally, the performance of a turbine is defined by a single parabolic performance curve, independent of inflow conditions and invariant in time. A unique maximum power-point exists for this condition and is achieved by maintaining a constant, optimal tip speed ratio (variable speed control). As a consequence of experimental blockage at a transitional Reynolds number, multiple

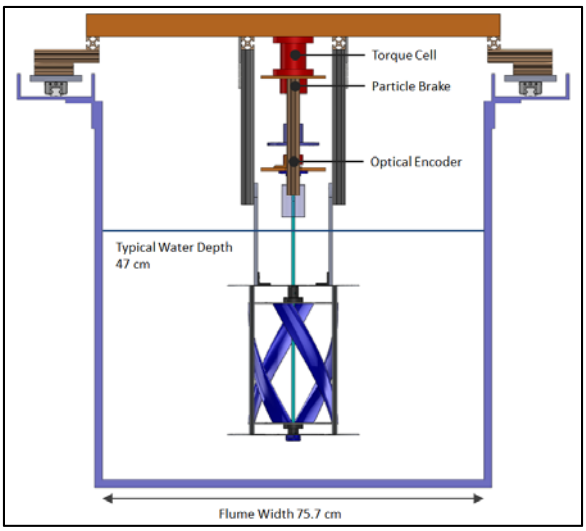

FIGURE 1. LAB SCALE TURBINE AND EXPERIMENTAL TEST RIG.

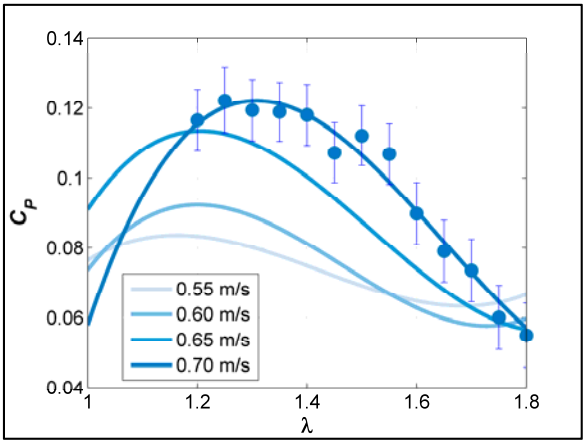

FIGURE 2. PERFORMANCE CURVES WITH TYPICAL EXPERIMENTAL SCATTER AND UNCERTAINTY SHOWN FOR AN INFLOW VELOCITY OF 0.7 M/S.

performance curves that are a function of inflow velocity exist for the laboratory scale turbine [8]. For a field-scale turbine, variable efficiency for balance of system components (e.g., gearbox, generator) may also produce a family of maximum power points with inflow velocity dependence [9]. Therefore, a controller that can adapt to a time-varying maximum power point is desirable.

A set of idealized performance curves for inflow velocity ranging from 0.55 m/s to 0.70 m/s are shown in Figure 2. Third-order polynomials are fit to the experimental data to obtain continuously differentiable curves. Optimal C_P and corresponding λ estimates are approximated as a linear function of inflow velocity.

Disturbance Characteristics

As inflow velocity cannot be controlled in a natural environment, it is considered to be a variable disturbance to the system. A series of velocity profiles (Figure 3) are obtained by

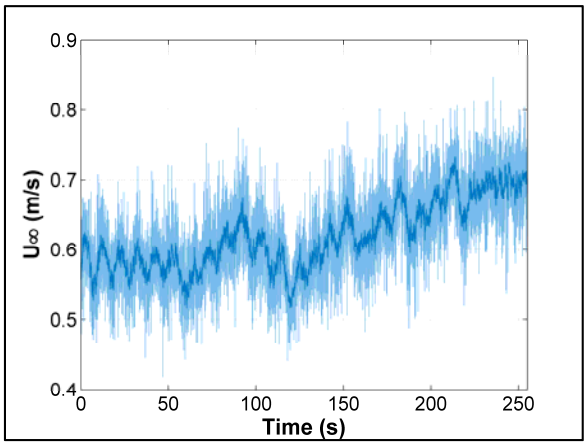

FIGURE 3. TYPICAL INFLOW VELOCITY FOR CONTROLLER VALIDATION, RAW (FINE LINE, 100 HZ) AND SMOOTHED (10 HZ).

manually keying the flume pump controller through a pre-determined sequence. Current velocity is measured using the analog output from a Nortek Vector ADV and post-processed to remove statistical outliers [10]. Though each test comprises an independently performed experiment with slightly different time series, the inflow conditions and velocity acceleration is similar for all experiments. The velocity measurements are not smoothed for use in the control schemes to allow the controller to attempt to react to turbulence at all measured scales.

Experimental Control Strategies

The experimental turbine is fixed pitch, but its rotation rate can be adjusted by varying the voltage supplied to the particle brake. The dynamics of the turbine are modeled in the following treatment as

$$\dot{\omega} = \frac{1}{J}(\tau - \tau_c) \tag{3}$$

where J is the rotational inertia of the turbine. Hydrodynamic and control torque are equal when the turbine's rotation rate is steady. Three variations on a nonlinear "torque control" scheme are evaluated for their ability to optimize mechanical power generation. In order of increasing complexity, these variations are constant gain control, feedforward adaptive gain control, and hybrid feedback/feedforward adaptive gain control.

For all three schemes, the control torque is related to peak C_P at a corresponding λ_* as

$$\tau_c = \left(\frac{1}{2}\rho A R^3 \frac{C_{P_{max}}}{\lambda_*^3}\right)\omega^2 = K\omega^2 \tag{4}$$

where K is the control law gain [11]. Dependence on ω^2 and the ideally parabolic nature of the characteristic curves imply that the control schemes are all nonlinear. In the case of a unique maximum power point, K is time invariant. Linearizing C_{Pmax} and λ_* as functions of velocity for the experimental performance curves (Figure 2), the adaptive gain, defined as K^*, becomes

$$K^* = \frac{1}{2}\rho A R^3 \frac{[0.273U_\infty - 0.068]}{[0.920U_\infty + 0.645]^3} \tag{5}$$

and is a nonlinear function of inflow velocity (U_∞). The control torque is dominated by the ω^2 term, which is on the order of 10^2, while the gain (K) is on the order of 10^{-4}. Therefore, slight changes in the inflow velocity (and, subsequently, K for adaptive schemes) are expected to have limited effect on control torque command, as ${}^{dK}/_{dU_\infty} \sim 10^{-4}$.

Control schemes are evaluated by comparing the average power produced during an experiment to the power that would result from the turbine operating at C_{Pmax} for the same experimental velocity time series. The ratio of these quantities forms a non-dimensional term (P_{loss}) as

$$P_{loss} = 1 - \frac{\bar{P}_{actual}}{\bar{P}_{ideal}}. \tag{6}$$

This evaluation method assumes previously derived performance curves perfectly define optimal performance points, when in actuality, there is considerable uncertainty (~10% of C_P) associated with them. Consequently, for the experimental measurements it is possible for the actual performance to exceed the "ideal" performance. This is not the case for the numerical simulations described later in this paper.

Each control strategy is implemented in LabVIEW. A Virtual Instrument (VI) is created to collect angular position, torque, and inflow velocity utilizing a data acquisition board (National Instruments USB-6341) at a sampling rate of 100 Hz. The sampling rate is chosen to enable measurement of the turbulent fluctuations of inflow velocity on a small time-scale. Moving average smoothing of the previous 10 samples is performed on calculations of ω prior to computation of the control torque setpoint to reduce short-term variability in ω. τ_c is computed at each time step utilizing ω and, for some schemes, U_∞ measured at the beginning of the time step. Control actions are accomplished by setting the voltage level of the particle brake (Placid Industries B2-12-1) power supply. The voltage command is set to saturate at 4 V, introducing an element that provides robustness for strong perturbations

associated with spikes in ω or U_∞. A higher saturation voltage can cause the turbine to stall if control torque is suddenly elevated.

All measured quantities, including the control command, are recorded for post-processing in MATLAB to calculate P_{loss}. The dynamic response of the controlled turbine is characterized by computing power spectra for the inflow power and mechanical power output. Time series from each test are divided into ~20-second windows with 50% overlap before applying a fast Fourier transform with a Hamming filter.

Constant Gain Control Implementation

The simplest of the controllers, constant gain (Figure 4), is implemented by computing a value for K from a single characteristic maximum power point corresponding to a velocity of 0.63 m/s using (5) (average velocity for the experimental sequence). Torque command is a nonlinear function only of the measured turbine rotation rate. The applied torque is found to have a quadratic relationship to brake command voltage (determined in previous experimentation), which is solved for each loop iteration to obtain the appropriate voltage command. In the absence of torque feedback, this controller assumes the relationship between the brake command and actual applied braking torque is perfectly modeled.

Feedforward Adaptive Gain Control Implementation

For the feedforward with adaptive gain controller implementation (Figure 5), the previous scheme is modified to include velocity measurements in the computation of K. The gain is adapted based on upstream velocity (5).

Hybrid Feedback/Feedforward Control Implementation

The most complex of the controllers introduces a torque feedback loop, replacing direct brake control. The feedback loop ensures the torque commanded is achieved. At the beginning of each loop iteration, the control torque measurement is fed into a PI control VI where it is compared to the control torque setpoint. The control action sets the particle brake command voltage. Initially, a LabVIEW auto-tuning function is used to coarsely set PI gains. These gains are manually adjusted from their baseline values through a process of trial and error to maintain smooth rotation through all

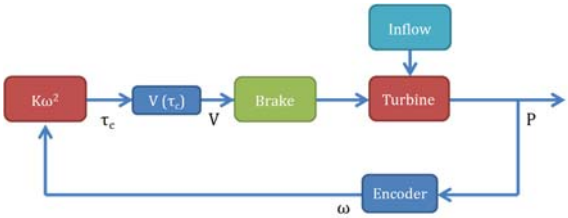

FIGURE 4. BLOCK DIAGRAM OF CONSTANT GAIN SCHEME.

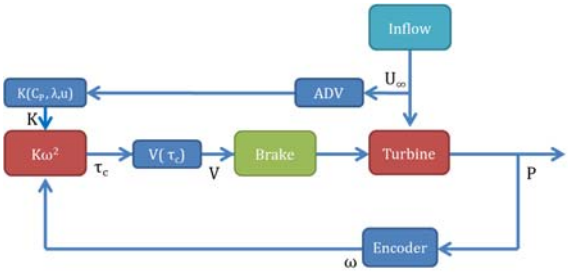

FIGURE 5. BLOCK DIAGRAM OF FEEDFORWARD ADAPTIVE CONTROL SCHEME.

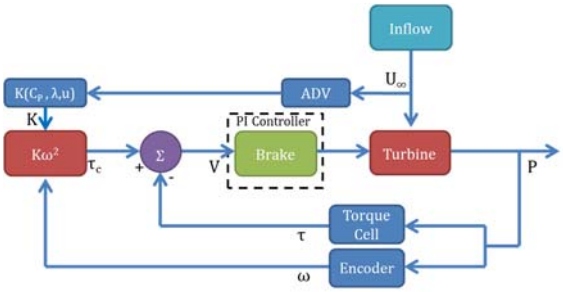

FIGURE 6. BLOCK DIAGRAM OF HYBRID CONTROL SCHEME.

operating conditions tested, including cut-in during a ramp-up of inflow velocity and cut-out during a ramp-down of inflow velocity. A block diagram depicting this control scheme is shown in Figure 6.

Numerical Simulations

The effectiveness of the control algorithms is also investigated with time-domain analyses of constant-speed control (i.e., constant rotation rate), feedfoward adaptive gain control, and constant gain control. For the constant-gain case, controller gain is simulated for the average velocity of the time series, as well as for poor guesses of velocity less than and greater than the mean. The idealized characteristic curves used to identify the maximum power point are also used for the control simulation (Figure 2). However, for simulation, two-dimensional interpolation is performed on the families of performance curves to calculate hydrodynamic performance and the controller gain at each time step. These curves define both the turbine performance and controller gain, whereas in the experiments, the

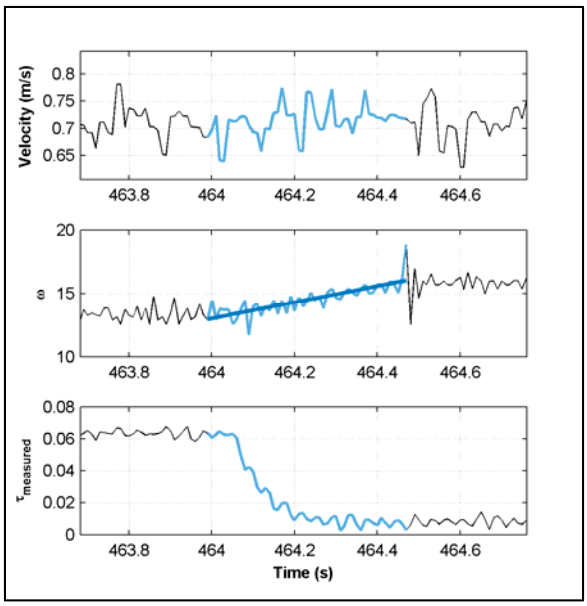

FIGURE 7. SYSTEM RESPONSE TO A STEP CHANGE IN CONTROL TORQUE. BLUE LINES DENOTE THE WINDOW USED TO ESTIMATE *J* FROM CHANGES IN *T* AND *Ω*.

controller gain is defined by the curves, but turbine performance can depart from these curves (i.e., the characteristic curves describe average, not instantaneous performance for the experiment).

Simulations are performed using a single, despiked velocity time series from the experiments. At time t = 0, the simulation is initialized with a rotation rate corresponding to optimal performance at the initial velocity. The simulation then steps through time (Δt = 0.005 s) with the turbine rotation rate evolving as

$$\omega_{i+1} = \omega_i + \dot{\omega}\Delta t \qquad (7)$$

where $\dot{\omega}$ and K are determined as for the experiments. For the constant rotation rate case, $\dot{\omega}$ is taken to be zero for all time. At each time step, both the power produced by the turbine and power that would have been produced if the turbine was operating at maximum efficiency is calculated and P_{loss} evaluated for the full time series.

The simulations require an estimate of the turbine's rotational moment of inertia (J). This is extracted from experimental data for a step change to the control torque under steady flow conditions (not part of the control scheme experiments described previously). The start and end times of the change in control torque are identified and the change in rotational rate estimated from a linear fit to the rotation rate measurements. For this calculation, it is assumed

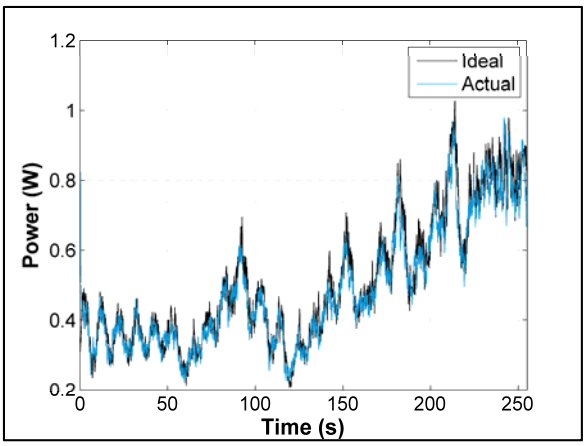

FIGURE 8. HYBRID CONTROLLER PERFORMANCE

that the turbine's hydrodynamic torque remains constant over the duration of the step change (< 0.5 s), such that τ_c is assumed to be the measured torque at the end of the step change and τ is assumed to be the measured torque at the beginning of the step change (at which point, τ_c and τ are balanced). The system response to a representative step change in shown in Figure 7. Ten such step changes in control torque are evaluated, resulting in an estimate of J = 1.1±0.2 kg m^2.

RESULTS

Experimental Controller Performance

Ideal power is compared against the actual power to evaluate controller performance. The time series for the hybrid controller (Figure 8) indicates the controller is successfully tracking target power, with a tendency to undershoot by a small amount (moving average smoothing over 0.5 seconds is performed for ease of visualization). Changes to the bulk flow (on the order of seconds) are handled well by the hybrid controller. The constant gain and adaptive gain feedforward controllers perform similarly, with a higher degree of undershoot. Power loss for the three controllers is summarized in Table 2. The hybrid controller outperformed both feedforward adaptive gain and constant gain control. Unexpectedly, constant gain control performs slightly better than feedforwad control with adaptive gain. This result may be a combination of uncertainty in the performance curves used to derive adaptive gain values and the control scheme's low sensitivity to changes in velocity. The improvement in performance due to the feedback loop of the hybrid control is attributed to this scheme's ability to ensure the commanded control torque is achieved – a feature absent in the other two controllers.

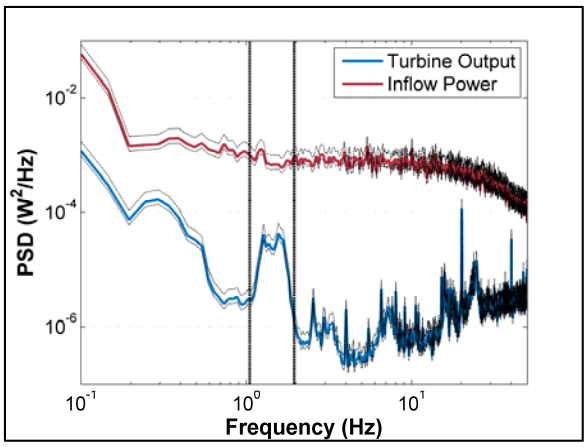

FIGURE 9. EXPERIMENTAL POWER SPECTRA WITH PRIMARY ROTATIONAL FREQUENCY RANGE (SOLID VERTICAL LINES).

Response to turbulent fluctuations at higher frequencies is evaluated by comparing the power spectra of turbine power output and inflow power (Figure 9). The range of turbine rotational frequency (between vertical lines) corresponds to a wide plateau in the power output spectra associated with control actions. A steep drop-off occurs beyond 1.8 Hz, indicating the system is non responsive to turbulence on time scales on the order of ~ 0.5 s or faster. The upward trend in the output power spectrum above 5 Hz is thought to be the product of experimental noise; the torque sensor is sensitive to high frequency vibration of the flume and test frame. All control schemes exhibit similar dynamic characteristics.

Numerical-Experimental Comparison

P_{loss} for each case is listed in Table 2. For the numerical simulations, turbine performance under feedforward control with adaptive gain is within a few percent of ideal performance. Because the controller gain is dominated by variations in ω^2, performance under constant gain control, even with a poor assumption for inflow velocity, is only somewhat worse than adaptive feedforward control. However, constant speed control performs significantly worse than any of the torque control simulations, reducing power generation by 21% relative to an ideal system in simulations.

DISCUSSION AND CONCLUSIONS

An adaptive gain control scheme for a laboratory-scale hydrokinetic turbine is successfully implemented, allowing the turbine to remain close to its maximum power point during inflow disturbance. The turbine performance is such that the maximum power point is close to stall conditions and PI controller gains need to be tuned to prevent stall for the hybrid scheme or

TABLE 2. P_{LOSS} FOR EXPERIMENTS AND SIMULATIONS

	Experiment	Simulation
Constant speed	N/A	21%
Constant gain		
U_{guess} = 0.63 m/s	11%	3%
U_{guess} = 0.5 m/s	N/A	5%
Feedfoward, adaptive gain	12%	2%
Feedback/Feed-forward, adaptive gain	4%	N/A

allowed to saturate for feedforward control. This is a particular challenge for turbines operating at relatively low tip-speed ratios as a stalled turbine obviously produces no power and may suffer cumulative damage from an increase in the number of start-up cycles over its lifetime. For these experiments, limiting the control torque is able to mitigate this problem.

It is shown that the system reacts to turbulence over time scales no faster than a few Hz, indicating a controller sampling rate of 10-20 Hz would be as effective for maximizing power production. Slower controller response may also limit the potential for high-frequency control torque adjustments that could damage a turbine drive train. The plateau observed in the power spectrum for output power in the range of turbine rotational frequency may be indicative of variable speed control maximizing performance over a range of rotational rates. Chammoro et al. [12] tested a horizontal-axis laboratory scale turbine at constant rotation rate and observed a strong deviation of power output from tracking inflow velocity above single-valued rotational frequencies.

Experiments to control the laboratory-scale cross-flow turbine and time-domain simulation suggest that torque control can substantially improve performance relative to constant speed control, with additional, incremental benefits from adaptive gain and feedback. The turbine considered in this investigation has a low moment of inertia and a family of characteristic performance curves that are a function of inflow velocity. For other systems (e.g., larger turbine with a greater moment of inertia and a characteristic performance curve independent of velocity), the benefit from torque control with preview information may differ. However, there are several situations of practical interest that may lead to families of performance curves similar to those investigated here. One, as noted previously, can occur when the coupling of the turbine rotor to the drive train produces a family of overall performance curves due to variations in balance of

system efficiency (e.g., gearbox, generator). A second case corresponds to community-scale turbines (i.e., rated power output on the order of 10 kW) operating at a transitional Reynolds number. A third corresponds to arrays of large tidal turbines operating at high blockage for performance augmentation [13,14]. In the latter case, the characteristic performance of each turbine in the array would likely vary with local inflow velocity.

Though adaptive control is shown to have limited efficacy at improving energy capture experimentally, value is seen in testing control schemes at this scale. Turbine stall, sensor noise, the effects of blockage, and operation in a transitional Reynolds regime are difficult to simulate numerically and the robustness of a scheme can be investigated experimentally before being enacted in the field.

Experiments with the described control techniques are presently only used for Region 2 control where performance optimization is the goal. Preview-based methods may also have utility for Region 3 control, where maintaining operation at rated power is the goal, and for smooth transitions between these regions. The latter objective appears promising, as abrupt changes to the control method can be eliminated by anticipating switches to and from constant power output, obviating the need for a separate "Region 2.5" control scheme [6]. While Region 3 torque control is not considered viable for axial flow turbines due to the high, fluctuating loads this places on the drive train components, Region 3 torque control may be viable for cross-flow turbines given their lower rotational moment of inertia.

Encoder measurement derived rotation rate feedback is utilized and required smoothing to be useful for control. Experimentation with increased rotation rate smoothing and smoothing of the torque feedback have not yet been conducted, but are candidates for future work. Additionally, future work will involve implementation of *in situ* system identification and a model-following controller [15,16]. The ultimate goal is to forgo utilizing pre-processed characteristic performance curves to determine optimal controller setpoints. As shown by the comparison of experimental results to the analytical simulation, the instantaneous uncertainty in these curves presents a challenge to controller optimization. Additionally, characteristic performance is likely to change over extended deployment due to bearing wear, temperature change, and biofouling (micro- and macro-scale). The ability of a controller to maximize efficiency for a changing system is one pathway towards reducing the levelized cost of energy for hydrokinetic energy systems.

ACKNOWLEDGEMENTS

The authors wish to acknowledge the financial support of the US Department of Energy under DE-FG36-08GO18179-M001, the University of Washington Royalty Research Fund, and fellowship support for Robert Cavagnaro provided by Dr. Roy Martin. Thanks also to Caleb Bowman, Fiona Spencer, Eamon McQuaide and Kevin Soderlund for engineering and facilities support.

REFERENCES

1 Güney, M. S., & Kaygusuz, K. (2010). Hydrokinetic energy conversion systems: A technology status review. *Renewable and Sustainable Energy Reviews*, *14*(9), 2996–3004. doi:10.1016/j.rser.2010.06.016

2 Benelghali, S., El, M., Benbouzid, H., Member, S., & Charpentier, J. F. (2012). Generator Systems for Marine Current Turbine Applications : A Comparative Study, *37*(3), 554–563.

3 Vallet, M. A., Bacha, S., Munteanu, I., Bratcu, A. I., & Roye, D. (2011). Management and Control of Operating Regimes of Cross-Flow Water Turbines. *IEEE Transactions on Industrial Electronics*, *58*(5), 1866–1876. doi:10.1109/TIE.2010.2058073

4 Birjandi, A. H., Woods, J., & Bibeau, E. L. (2012). Investigation of macro-turbulent flow structures interaction with a vertical hydrokinetic river turbine. *Renewable Energy*, *48*, 183–192. doi:10.1016/j.renene.2012.04.045

5 Ginter, V. J., & Pieper, J. K. (2011). Robust Gain Scheduled Control of a Hydrokinetic Turbine. *IEEE Transactions on Control Systems Technology*, *19*(4), 805–817. doi:10.1109/TCST.2010.2053930

6 Laks, J., Pao, L., Wright, A., Kelley, N., & Jonkman, B. (2011). The use of preview wind measurements for blade pitch control. *Mechatronics*, *21*(4), 668–681. doi:10.1016/j.mechatronics.2011.02.003

7 Wang, N., Johnson, K. E., & Wright, A. D. (2012). FX-RLS-Based Feedforward Control for LIDAR-Enabled Wind Turbine Load Mitigation. *IEEE Transactions on Control Systems Technology*, *20*(5), 1212–1222. doi:10.1109/TCST.2011.2163515

8 Cavagnaro, R., Polagye, B. An investigation into blockage corrections for cross-flow hydrokinetic turbine performance [abstract]. In: 66th Annual Meeting of the APS Division of Fluid Dynamics Volume 58, Number 18.; November 24-26, 2013; Pittsburgh, Pennsylvania. Session A13: Focus Session: Marine Hydrokinetic Energy Conversion I, A13.00003.

9 Polagye, B., R. Cavagnaro, and A. Niblick (2013) Micropower from Tidal Turbines, ASME Fluids Division Summer Meeting, July 8-11, 2013, Incline Village, NV.

10 Mori, N., T. Suzuki and S. Kakuno (2007) Noise of acoustic Doppler velocimeter data in bubbly flow, Journal of Engineering Mechanics, American Society of Civil Engineers, Vol.133, Issue 1, pp.122-125. (doi:10.1061/(ASCE)0733-9399(2007)133:1(122))

11 Johnson, K. E. (2004). *Adaptive Torque Control of Variable Speed Wind Turbines Adaptive Torque Control of Variable Speed Wind Turbines*. National Renewable Energy Laboratory, Golden Colorado. doi:NREL/TP-500-36265

12 Chamorro, L. P., Hill, C., Morton, S., Ellis, C., Arndt, R. E. a., & Sotiropoulos, F. (2013). On the interaction between a turbulent open channel flow and an axial-flow turbine. *Journal of Fluid Mechanics*, *716*, 658–670. doi:10.1017/jfm.2012.571

13 Whelan, J. I., Graham, J. M. R., & Peiró, J. (2009). A free-surface and blockage correction for tidal turbines. *Journal of Fluid Mechanics*, *624*(March 2009), 281. doi:10.1017/S0022112009005916

14 Garrett, C., & Cummins, P. (2007). The efficiency of a turbine in a tidal channel. *Journal of Fluid Mechanics*, *588*, 243–251. doi:10.1017/S0022112007007781

15 Freeman, J. B., & Balas, M. J. (1999). An Investigation of Variable Speed Horizontal-Axis Wind Turbines Using Direct Model-Reference Adaptrive Control (pp. 66–76). American Institute of Aeronautics and Astronautics, Reston, VA. doi:10.2514/6.1999-28

16 Schlipf, D., Schlipf, D. J., & Kühn, M. (2013). Nonlinear model predictive control of wind turbines using LIDAR, *Wind Energy*, 16, 1107–1129. doi:10.1002/we. 1533